Deactivation Mechanism of the Green Fluorescent Chromophore

Rinat Gepshtein,[†] Dan Huppert,[†] and Noam Agmon*[,‡]

Raymond and Beverly Sackler Faculty of Exact Sciences, School of Chemistry, Tel Aviv University, Tel Aviv 69978, Israel, and Department of Physical Chemistry and the Fritz Haber Research Center, The Hebrew University, Jerusalem 91904, Israel

Received: July 20, 2005; In Final Form: December 22, 2005

We report time-resolved fluorescence data for the anion of *p*-hydroxybenzylidene dimethylimidazolinone (*p*-HBDI), a model chromophore of the green fluorescence protein, in viscous glycerol−water mixtures over a range of temperatures, *T*. The markedly nonexponential decay of the excited electronic state is interpreted with the aid of an inhomogeneous model possessing a Gaussian coordinate-dependent sink term. A nonlinear least-squares fitting routine enables us to achieve quantitative fits by adjusting a single activation parameter, which is found to depend linearly on $1/T$. We derive an analytic expression for the absolute quantum yield, which is compared with the integrated steady-state fluorescence spectra. The microscopic origins of the model are discussed in terms of two-dimensional dynamics, coupling the phenyl-ring rotation to a swinging mode that brings this flexible molecule to the proximity of a conical intersection on its multidimensional potential energy surface.

1. Introduction

The green fluorescent protein (GFP) has attracted great interest as a biological fluorescence marker.[1−3] Its *p*-hydroxybenzylidene imidazolinone chromophore (Cro) forms posttranslationally by a cyclization reaction within a tripeptide unit (Ser65, Tyr66, Gly67). It is housed within the rigid 11 β-sheet barrel-like structure of the GFP, where it is anchored both covalently and via an extended hydrogen-bond (HB) network. Following photoexcitation,[4] this aromatic Cro undergoes a rapid reaction of excited-state proton transfer (ESPT), producing a brightly fluorescing anion, with a fluorescence quantum yield (QY) of about 0.8.

Interestingly, when the protein denatures it becomes nonfluorescent.[5] Model Cro's were consequently synthesized,[6−10] for example, *p*-hydroxybenzylidene dimethylimidazolinone (*p*-HBDI, Figure 1).[9,10] These dye molecules also proved to be very weakly fluorescent in room-temperature (RT) solvents (QY $< 10^{-3}$). However, they increase their quantum yield dramatically at 77 K. An important question thus arises, how does the protein convert such a poor fluorophore to the brightly fluorescent GFP? A clear answer to this question could assist in designing brighter GFP variants.

The difference in fluorescence efficiency is due to nonradiative processes that are curtailed by the rigid[11] barrel structure of GFP. One possibility is that the protein protects against diffusing quenchers (e.g., molecular oxygen) in solution.[1] This interpretation is inconsistent with the persistence of nonradiative decay of model Cro's in viscous solutions at low temperatures (T),[12] where quencher diffusion times become much longer than the nanosecond time scale of the nonradiative decay process.

Time-resolved spectroscopic measurements on these compounds[12−16] find ultrafast picosecond decay in RT solvents concomitant with ground-state (GS) recovery. This implicates noncollisional internal conversion (IC) as the underlying decay mechanism.[17] However, there is no agreement on the details of the mechanism. One group[13−15] performed femtosecond upconversion and pump−probe measurements on HBDI at RT, finding little dependence on solvent polarity and viscosity (up to 16 cP), thus excluding the participation of solvent-displacing rotations around the angles ϕ and ψ in Figure 1. Possibly only the concerted "hula-twist" motion is consistent with their data. (They also find little transient red shift but an observable line narrowing.) Another group[12] extended the measurements to very viscous solvents and low temperatures, finding strong viscosity dependence and concluding that rotation around one or both bonds leads to IC. (They also find inhomogeneous distributed decay kinetics, requiring up to four exponentials to fit the data.)

Quantum chemistry calculations[18−24] implicate the participation of a conical intersection[17] in the IC process within the GFP Cro. The ground (S_0) and excited (S_1) potentials in the (ϕ, ψ) coordinate system approach each other closely at certain configurations where facile IC is predicted to occur. However, even high-level calculations are at odds with respect to identifying the active mode that leads to the intersection (ϕ,[23] ψ,[24] or a concerted hula-twist[22]). It is not possible to say whether the transient fluorescence data support any of these scenarios, because a quantitative kinetic model has never been applied to the experimental data. The seemingly complex multiexponential kinetics[12] remains thus far uninterpreted.

A simple model for nonradiative decay via nonadiabatic curve-crossing (a one-dimensional version of a conical intersection) was suggested by Bagchi, Fleming, and Oxtoby (BFO).[25] At the intersection of the potential curves ($V_1(x)$ and $V_0(x)$ in Figure 2), and only there, rapid IC occurs. It is therefore described by a delta-function "sink term". After excitation to S_1, the distribution $p(x)$ has to diffuse to the intersection point to decay back to the GS. This suggests that at low viscosities the decay should begin with a delay, which has not been observed. In highly viscous solvents no IC should occur, because the distribution cannot diffuse to the intersection point. This

* Author to whom correspondence should be addressed. Phone: +972-2-6585687. Fax: +972-2-6513742. E-mail: agmon@fh.huji.ac.il.
[†] Tel Aviv University.
[‡] The Hebrew University.

10.1021/jp0540095 CCC: $33.50
Published on Web 02/14/2006

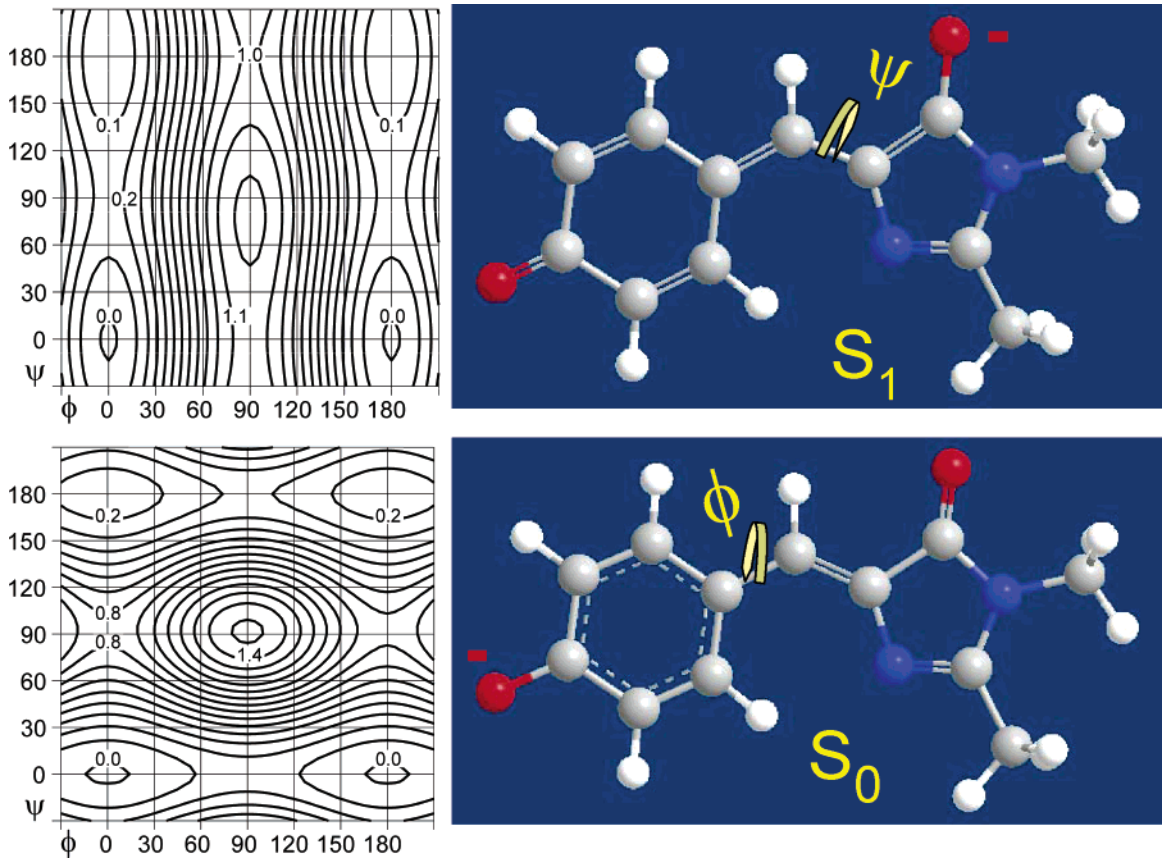

Figure 1. Right: Structure of the *p*-HBDI anion (optimized for the GS using the MM2 option of Chem3D, version 9.0, by CambridgeSoft), showing approximate single/double bonding patterns for the GS and ES and identifying the two exocyclic angles, ϕ and ψ. Color codes: hydrogen, white; carbon, gray; oxygen, red; and nitrogen, blue. The equilibrium geometry shown is planar. Left: Corresponding potential energy surfaces in these two angles, as calculated by Scharnagl and Raupp-Kossmann (reproduced with permission of the authors).[21] Contour spacing 0.1 eV. The (ϕ, ψ) equilibrium geometry in both electronic states is planar, (0, 0) or (180, 0).

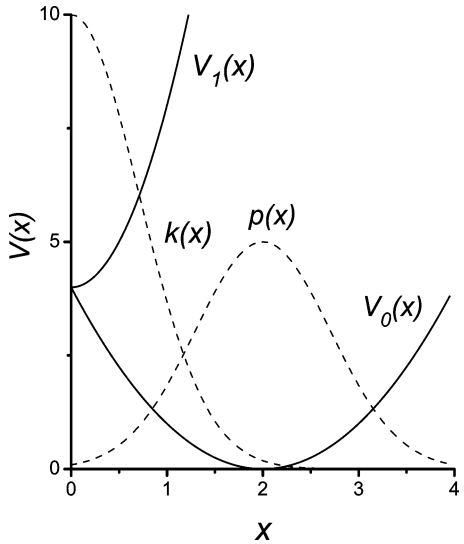

Figure 2. One-dimensional potential energy surfaces for an ultrafast ES isomerization reaction (bold lines), and the inhomogeneous model for ES decay (dashed lines). The potential curves demonstrate eq 1, with $x_0 = 2$, $\alpha_0 = 1$, and $\alpha_1 = 4$. The GS potential intersects the ES potential at its minimum. The conformational distribution, $p(x)$, and sink term, $k(x)$, demonstrate eqs 2 and 5 with arbitrary normalization. Thus only their x values are shared with the potential functions, $V_i(x)$.

expectation contradicts the experimental observation[12] of fast (nanosecond) multiexponential IC even in viscous solvents.

Hence within the curve-crossing picture, the sink term $k(x)$ must be nonlocal, allowing IC at a range of coordinates rather than at a single point. It is coupled to an inhomogeneous distribution in the same coordinate, which is transferred from the GS to the excited-state (ES) by the photoexcitation process. Clear evidence for inhomogeneous broadening comes from the shape of the steady-state fluorescence spectrum. While that of GFP is narrow and shows vibrational features,[2] the spectra of the model Cro's (which increase dramatically in intensity as T is lowered) are much wider and featureless.[12−14]

Inhomogeneous kinetics is also implicated in ligand binding to myoglobin in low-temperature glasses,[26] where a conformational distribution is coupled to an exponential sink term.[27−31] Recently it was shown that, in viscous solvents, a Gaussian sink fits the data better in both the static and the dynamic limits.[32] This allowed identification of the different relaxation modes and determination of their activation energies. Several of these modes turn out to be rotations around dihedral angles of amino acid side chains in the distal heme pocket. These motions are thus similar to the rotational modes discussed for HBDI.

It was also shown that a nonlocal sink term can arise from a second degree of freedom that is fast compared to the distributed mode.[27,28] Such a two-dimensional picture has been invoked for explaining the fractional viscosity dependence in stilbene isomerization.[33] For HBDI, two-dimensional potentials (in hypothetical coordinates) were postulated to play a role in its nonexponential kinetics.[15] Potential surfaces in the (ϕ, ψ) coordinates were recently calculated using quantum chemistry methods.[21] The anionic surfaces are reproduced in Figure 1. It is seen that the GS surface has a shallow potential for rotation around the single bond (ϕ) and a steep one for the double bond (ψ). In the ES, the roles of the two bonds invert as a result of the keto−enol tautomerization. The potential is now shallow

in ψ and steeply varying in ϕ. One can envision a wide GS distribution in ϕ that is frozen in viscous solutions. In the ES, it is assisted toward the conical intersection by fast librations in the ψ coordinate.

The present work is devoted toward developing a simple model for inhomogeneous ES decay due to IC. It is applied to the photodynamics of HBDI in low-temperature viscous solvents. We utilize basic solutions to maintain the dye in its anionic form and thus decouple it from ESPT that may occur at lower pH values. Using a Gaussian sink term, we are able to obtain exceptional fits by adjusting a single parameter with temperature. The quantitative agreement between experiment and theory provides direct support to the conical intersection mechanism for IC in a two-dimensional potential. The ϕ coordinate is frozen and inhomogeneously distributed, while a weakly activated libration in ψ assists the population in reaching the intersection region.

2. Theory

In this section we present a simple theoretical model for the kinetics of IC by conical intersection, to be applied here in the static limit of purely inhomogeneous kinetics. Thus we expect it to be applicable only in very viscous solvents, when no conformational relaxation takes place during the ES lifetime.

2.1. Potential. The model assumes a single floppy coordinate, x, governing the conformational state of the system. The potential in this coordinate is assumed to be harmonic for the two electronic states, S_0 and S_1, respectively (Figure 2):

$$V_0(x) = \alpha_0(x - x_0)^2$$

$$V_1(x) = \alpha_1 x^2 + \alpha_0 x_0^2 \quad (1)$$

We consider here the same barrierless situation as in the BFO model,[25] where the GS potential intersects the ES potential at its minimum. For simplicity we consider the regime where $x \geq 0$.

The V_i are not simple potential functions, because they implicitly include the coupling to all other degrees of freedom and to the solvent. Thus they are actually Gibbs free energies, in which the α_i may be temperature-dependent. Here we make the simple assumption that α_0 is proportional to k_BT (k_B is Boltzmann's constant). This type of behavior is typical of rubber elasticity.[34] It has also been suggested for the protein coordinate in heme protein kinetics.[30] It arises from coupling to other degrees of freedom that are entropic in nature, with the number of coupled coordinates increasing with T. Thus the slow, large-amplitude mode of the system (x) has elastic characteristics, which possibly result from its strong coupling to the solvent. This assumption will be justified retrospectively, when we find (below) that the $k(x)$ obtained from it obeys the physically reasonable Arrhenius temperature dependence.

For simplicity, we choose the units of x to eliminate the proportionality constant, so that $\alpha_0 = k_BT$. This simplifies the Boltzmann equilibrium distribution, which presumably prevailed in $V_0(x)$ prior to excitation

$$p(x) = Z \exp[-V_0(x)/k_BT] = Z \exp[-(x - x_0)^2] \quad (2)$$

Z is its normalization constant. This inhomogeneous distribution for the slow (here−frozen) coordinate is thus invariant of both temperature and time.

2.2. Deactivation Rate. Transitions from S_1 to S_0 can occur by two photophysical processes. The radiative process is homogeneous, with the same radiative lifetime, τ_f, for all conformations. In contrast, the nonradiative (nr) process is inhomogeneous. Thus instead of having a single rate constant, k_{nr}, each conformation x decays back to the GS by its own rate constant, $k(x)$.

We assume that $k(x)$ obeys an "energy-gap law"[35,36]

$$k(x) = A \exp(-\gamma \Delta V(x)/k_BT) \quad (3)$$

Here A is a preexponential with units of 1/time, and γ is a characteristic parameter. In the language of radiationless transitions,[36] there are two limits where an analytic expression for the nonradiative rate constant, k_{nr}, can be worked out. In the strong-coupling regime the shift between the minima of the two potentials is large and k_{nr} shows a Gaussian dependence on their (nonvertical) energy difference, ΔE. In the weak coupling limit the two potentials have their minima at nearly the same location, and k_{nr} depends exponentially on ΔE (which in this limit is the *vertical* energy difference).

In our case one coordinate, x, is in the strong-coupling regime, but we assume that it is frozen. The remaining coordinates are in the weak coupling limit; hence their energy difference depends on the value of the slow coordinate, x. It is given by

$$\Delta V(x) = V_1(x) - V_0(x) = (\alpha_1 - \alpha_0)\, x^2 - 2\alpha_0 x_0\, x \quad (4)$$

This expression encompasses the two limits, exponential and Gaussian, previously considered for the dependence of $k(x)$ on x: (i) If the curvatures in the two states are equal, $\alpha_1 \approx \alpha_0$, then $k(x)$ is an exponential function of x as in refs 27 and 28. (ii) If $\alpha_1 \gg \alpha_0$, then $k(x)$ is a Gaussian as in ref 32. The present system belongs to the second case, where $\Delta V(x) \approx \alpha_1 x^2$. Thus setting $b \equiv \alpha_1\gamma/k_BT$ in eq 3, we obtain a Gaussian sink term of the form

$$k(x) = A \exp(-bx^2) \quad (5)$$

As we shall see below, the only temperature-dependent term in this model is b.

2.3. Transient Fluorescence. In the static limit, the probability $P(t)$ that the ES has not decayed by time t after excitation is given by

$$P(t) = \exp(-t/\tau_f) \int_0^\infty p(x) \exp[-k(x)t]\, dx \quad (6)$$

The first exponential accounts for the homogeneous radiative decay process, whereas the integral of the second exponential represents the inhomogeneous nonradiative decay kinetics. We reiterate that this simple result is valid only in the viscous glassy environment considered herein, when no conformational dynamics takes place.

The observed transient fluorescence signal, $I(t)$, is consequently a convolution of the instrument response function (IRF), $I_0(t)$, with the theoretical decay function

$$I(t) = Z_0 \int_{-\infty}^{t} P(t - t')I_0(t')\, dt' \quad (7)$$

where Z_0 is a normalization constant for $I_0(t)$.

2.4. Steady-State Fluorescence. Finally, we derive an expression for the absolute fluorescence QY, $Q(T)$. It is defined as the fraction of excited molecules that decay radiatively by the emission of a photon. Since the latter is a unimolecular process, its transient rate is given by $\tau_f^{-1}P(t)$. The absolute QY is the time integral of this rate

$$Q(T) \equiv \int_0^\infty \tau_f^{-1} P(t)\, dt = \langle \tau \rangle / \tau_f. \quad (8)$$

The second equality suggests that $Q(T)$ can also be interpreted as the ratio of the average ES lifetime

$$\langle \tau \rangle \equiv \int_0^\infty P(t)\, dt$$

and the radiative one.

The time integral in eq 6 can be performed analytically. Hence we find that for a static inhomogeneous process

$$Q(T) = \int_0^\infty \frac{p(x)}{1 + \tau_f k(x)}\, dx \quad (9)$$

$k(x)$ is given by eq 5, and it is the only term in the integrand that depends on T. Utilizing the fact that $k(x)$ is a rapidly varying function, one may approximate the spatial integral by replacing the denominator by a Heaviside function at a point $\bar{x}$. Defining $\bar{x}$ by $\tau_f k(\bar{x}) \equiv 1$, we assume that when $x < \bar{x}$ the denominator is so large that the integrand vanishes, whereas when $x > \bar{x}$ then $k(x) \ll 1$ and the integrand reduces to $p(x)$. Thus we obtain

$$Q(T) \approx 1 - \frac{1}{2} \mathrm{erfc}(x_0 - \bar{x}) \quad (10)$$

where erfc(z) is the complementary error function and

$$b\bar{x}^2 = \ln(A\tau_f) \quad (11)$$

This approximation is useful when $\bar{x}$ is small, in the rapidly varying shoulder of the Gaussian sink (e.g., $\bar{x} \approx 0.5$ in Figure 2). This is the limit when $Q(T)$ is close to unity. Thus for HBDI we expect eq 10 to apply at low temperatures.

3. Methods

3.1. Experimental Procedure. *p*-HBDI has been synthesized by standard methods[9,10] and characterized spectroscopically. These results are reported elsewhere.[37] *p*-HBDI was dissolved in water−glycerol mixtures of glycerol mole fractions $\chi_{gly} =$ 0.5, 0.4, and 0.2 using filtered water (resistivity > 10 MΩ) and glycerol (99% pure) from Aldrich. The pH of the solution was ≥10. Samples were placed in a 1 mm optical path length quartz cell. Its temperature was controlled by a liquid nitrogen cryostat with a thermal stability of approximately ±1 K.

Time-resolved fluorescence was acquired using the time-correlated single-photon counting (TCSPC). For excitation we used a cavity dumped Ti:sapphire femtosecond laser (Mira, Coherent), which provides short pulses (80 fs), operating at the SHG frequency (spectral range of 380−400 nm) and a relatively low repetition rate (500 kHz). The excitation pulse energy was reduced by neutral density filters to about 1 pJ. The TCSPC detection system is based on a Hamamatsu 3809U photomultiplier and an Edinburgh Instruments TC900 computer module for TCSPC. The overall scale was 20 ns, divided into 4096 channels, and the maximal count was typically around 10 000.

The instrumental response function (IRF), shown in Figure 3, was measured by front-end reflection from a liquid-filled cell that did not contain any fluorescent sample. It has a width of about 25 ps (fwhm) at RT, which increases below 200 K to 43 ps. This is due to enhanced diffusive scattering from the low-temperature glass. Due to the difference in measuring conditions between the IRF and the sample, the IRF is typically narrower than it should be. We corrected for this empirically, by widening the rising phase of the IRF by 50%. Time $t = 0$ was set at the peak of the IRF, and negative times were multiplied by a factor 1.5.

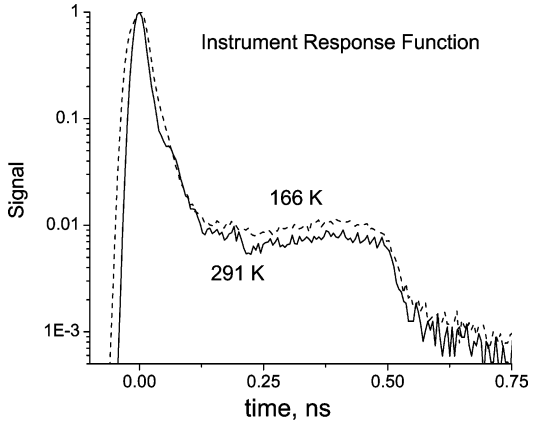

Figure 3. IRF for the TCSPC system at two temperatures, measured for a cell containing a 0.5 mol fraction glycerol in water. Note the logarithmic scale. The secondary peak around 400 ps leads to an apparent discontinuity of the high-temperature data (Figures 4 and 5).

For the actual measurements, $t = 0$ was set at two-thirds of the rising phase, and we allowed for a "jitter" of ±1 channel in the fitting procedure described below. The last 1 ns of the data was eliminated. We also deleted long-time tails when they reached the single-count limit and diluted the remaining data points.

3.2. Numerical Analysis. In the analysis and interpretation of the experimental data, much depends on numerical tools enabling an accurate theoretical fit to the data. A Fortran routine was written to perform a nonlinear least-squares fit of eqs 6 and 7 to the transient fluorescence data. The routine adjusts the two theoretical parameters, A and b in eq 5, as well as the normalization factor Z_0. A variant of the program allows us to keep A constant and adjust only b and Z_0.

Efficient convergence to a true global minimum is greatly aided by applying a combination of the gradient and Hessian methods.[38] To implement this option, the first and second (partial) derivatives of our fitting function (as a function of the fitting parameters Z_0, b, and A) were first obtained *analytically*, then read into the program.

The two integrals in eqs 6 and 7 were performed numerically during each iteration step in the calculation of the function and its derivatives. The spatial integration in eq 6 was done by simple series addition on an evenly spaced 80-point grid. The center of the GS potential in eq 1 was arbitrarily set at $x_0 = 2$, and integration was performed over the interval [0,4]. Temporal integration in eq 7 used the experimental TCSPC grid on which the IRF is defined.

The radiative lifetime τ_f was selected manually, and the quality of fit was utilized in verifying our choice. We also varied manually the jitter in setting $t = 0$ (see above), in an effort to further improve the fit at short times.

4. Results

4.1. Time-Resolved Fluorescence. The ES decay of the anionic HBDI dye was measured by time-resolved fluorescence in three water−glycerol mixtures over a temperature range of more than 100 K. The experimental data points are shown in Figures 4 and 5. The experimental fluorescence signal, $I(t)$, was multiplied by $\exp(t/\tau_f)$ so what is seen in the figures is the contribution from the pure nonradiative process. In the first figure we show the data on both linear and log−log scales,

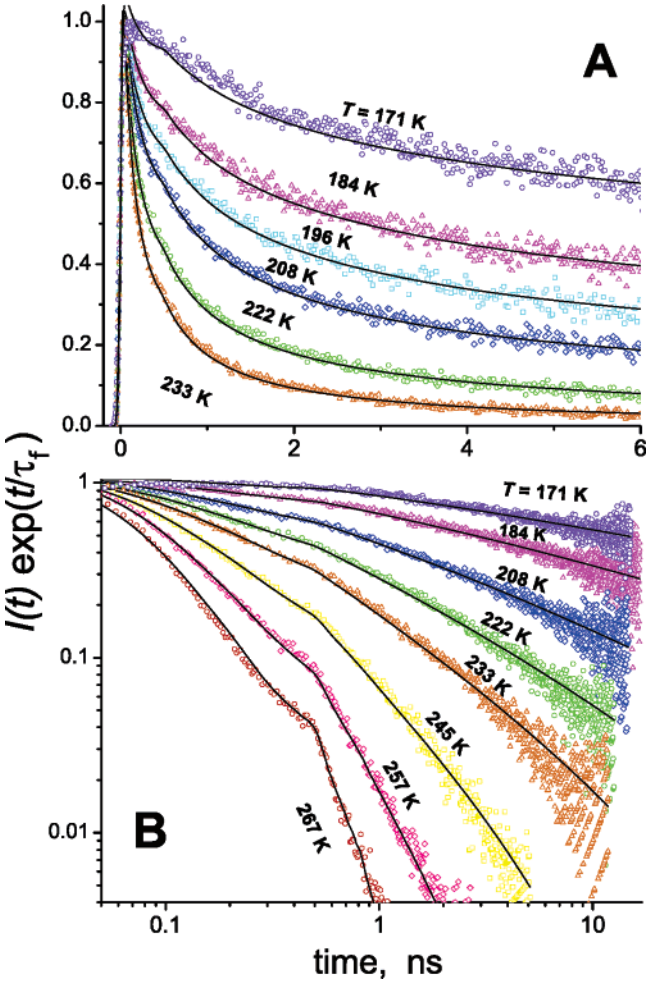

Figure 4. Radiationless decay of an excited *p*-HBDI dye in a 0.5 mol fraction glycerol−water mixture at various temperatures (indicated). The observed fluorescence signal was corrected for its radiative decay with a lifetime $\tau_f = 3.2$ ns. The sample was excited at 395 nm, and the fluorescence was collected at 530 nm, with a 10 nm bandwidth. (A) Linear short-time scale; (B) Long-time log−log scale. Points are experimental data, and lines are fits to the theoretical model obtained by adjusting *b*; see Table 1. Temperature-independent parameters: $A = 48$ ns^{-1}, $x_0 = 2$.

whereas the second figure utilizes only the log−log scale. The linear scale emphasizes the short-time behavior including the rise near $t = 0$ due to the excitation process. The log−log scale emphasizes the long-time behavior. An exponential decay with a fixed nonradiative rate constant, k_{nr}, would appear on this scale nearly flat at short times with a rapid drop at $t \approx 1/k_{nr}$. The much milder variation with t thus represents a distributed, multiexponential decay. This is not often encountered in simple dye molecules and thus requires a theoretical explanation.

A multiparameter nonlinear least-squares fit to the theoretical model was achieved using the software described above. τ_f was set to 3.2 ns for $\chi_{gly} = 0.5$ and to 3.4 ns for the other two solvents. These values are similar to the lifetime of the deprotonated form of wild-type GFP, 3.3 ns.[4] Since fits at different temperatures yielded similar *A* values for eq 5, we kept it constant at $A = 48$ ns^{-1}. The program was then run with only one theoretical adjustable parameter, *b* of eq 5, in addition to the normalization constant, Z_0. The latter is required by the finite width of the IRF and not because of theoretical considerations. Another IRF-induced artifact is the apparent discontinuity seen in the log−log scale at the high temperatures (Figures 4B and 5). It is due to the small secondary laser pulse around 400 ps (Figure 3).

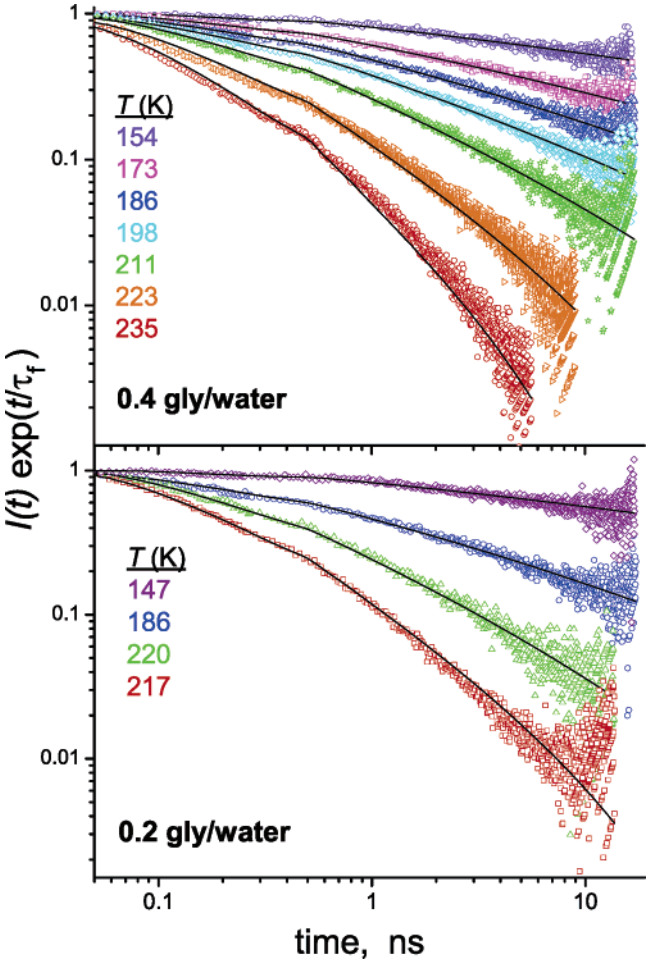

Figure 5. Same as Figure 4 for solutions of lower glycerol mole fractions on a log−log scale. Temperature-independent parameters: $\tau_f = 3.4$ ns, $A = 48$ ns^{-1}, $x_0 = 2$.

TABLE 1: Temperature Dependence of the Fitting Parameter in the Three Water−Glycerol Mixtures[a]

χ_{gly}					
0.5		0.4		0.2	
$\tau_f = 3.2$ ns		$\tau_f = 3.4$ ns		$\tau_f = 3.4$ ns	
T (K)	*b*	*T* (K)	*b*	*T* (K)	*b*
171	1.41	154	1.47	147	1.55
184	1.08	173	1.01	186	0.816
196	0.922	186	0.838	202	0.545
208	0.765	198	0.708	217	0.419
222	0.594	211	0.577		
233	0.482	223	0.436		
245	0.355	235	0.339		
257	0.265				
267	0.202				
282	0.16?				

[a] Global Parameters: $x_0 = 2$ and $A = 48$ ns^{-1}.

The fits are shown by the continuous lines in the figures, with the values of *b* collected in Table 1. They are excellent on all time scales, from the rising phase (Figure 4A) and up to the long-time low-amplitude tail, over 2 orders of magnitude in $I(t)\exp(t/\tau_f)$ (over 3 orders of magnitude for the raw data, $I(t)$). In comparison, the empirical four-exponential fit in ref 12 corresponds to a three-exponential fit to the nonradiative decay curves in our figures. Such fits utilize 6 adjustable parameters (time constants and amplitudes), as opposed to the single adjustable parameter of the present theoretical model. This clearly indicates

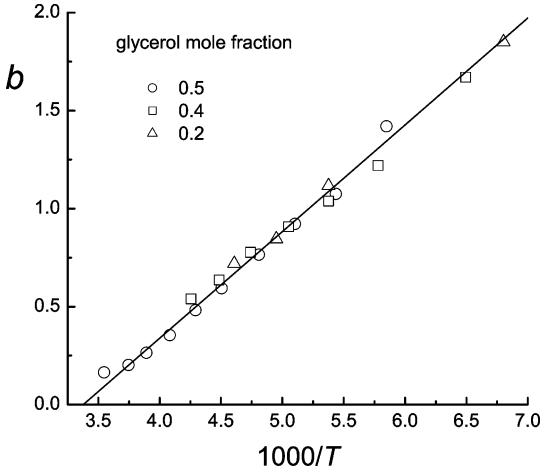

Figure 6. Temperature dependence of the parameter b obtained by fitting the data in Figures 4 and 5 (Table 1). The b values for $\chi_{gly} = 0.4$ and 0.2 were shifted upward by 0.2 and 0.3, respectively, to place them on the same straight line. Its equation is $-1.84 + 0.544(1000/T)$.

that our simple model represents a fundamentally sound physical description of the nonradiative decay process.

Some problems for the model are observed only at very low and high temperatures. In the very low temperature regime the signal seems to rise with a delay (see the 171 K data in Figure 4A). At least part of this is due to the slower decay of the IRF at the low temperatures, which arises from a stronger scattering of the glassy medium (Figure 3). At high temperatures the kinetics becomes too fast for our TCSPC apparatus and is expected to show dynamic (relaxation) effects, which are not covered by the present analysis.

Figure 6 depicts the temperature dependence of b. For $\chi_{gly} = 0.4$ and 0.2 it was shifted by a small constant (see legend), so that all points fall on a universal linear behavior

$$b = b_0 + b_1/T \tag{12}$$

This implies that the sink term in eq 5 has an Arrhenius-like temperature dependence

$$k(x) = [A \exp(-b_0x^2)] \exp(-b_1x^2/T) \tag{13}$$

for every fixed value of x. Hence A and b_1 are independent of the solvent whereas b_0 shows a weak solvent dependence. (However, part of the solvent-induced variation in b_0 compensates for differences in the τ_f values used herein). Because $b_0 < 0$, the preexponential frequency factor, $A\exp(-b_0x^2)$, *increases* from 4.8×10^{10} s^{-1} at $x = 0$ to 7.5×10^{13} s^{-1} at $x = x_0 = 2$. The activation energy, $k_Bb_1x^2$, increases from 0 to 18 kJ/mol over the same conformational range.

To check whether the kinetics are distributed not only in time but also in wavelength (λ), we present in Figure 7 the decay at the peak of the anionic HBDI emission (500 nm) and its two wings. At the two low temperatures, the faster decay of the blue wing can be explained by wavelength dependence of τ_f. We find that $\tau_f \propto \lambda$, which is weaker than the λ^3 dependence suggested for coumarin dyes.[39] (The 500 nm data is slightly overcorrected by this procedure, but using λ^3 would result in a poorer coincidence of the three data sets). Above 240 K, this correction does not suffice, which we interpret as evidence for the onset of relaxation in our x coordinate.

4.2. Steady-State Fluorescence. We test eq 9 for the absolute QY in Figure 8 (bold line). There are no adjustable parameters here, because we use those that were determined from the fit to

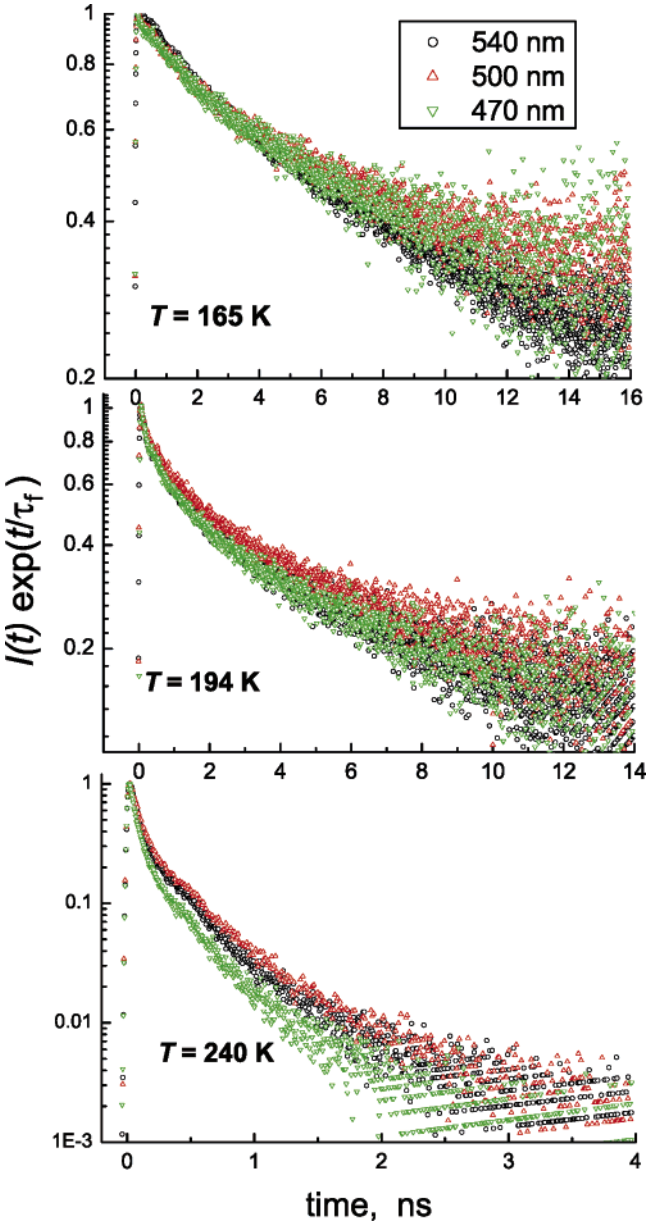

Figure 7. Wavelength dependence of anionic HBDI fluorescence in a 0.5 mol fraction glycerol−water mixture at the three indicated temperatures. The radiative lifetime is assumed proportional to λ: $\tau_f = 3.13$, 3.33, and 3.60 ns for $\lambda = 470$, 500, and 540 nm, respectively.

the transient data. It is compared, on one hand, to the analytic approximation in eq 10 (dashed line). As anticipated, this approximation performs well at low temperatures, when $Q(T) \approx 1$, but not at high T, when $Q(T)$ drops below 10% of its maximal value. On the other hand, we compare it to the relative QY obtained from the temperature dependence of the steady-state fluorescence spectra,[37] by either integrating the ν^3-scaled line shape as a function of frequency, ν,[40] or from the peak intensity. Both methods give similar results, which are shown as the points in Figure 8. The agreement with eq 9 is good at low T but deteriorates as the sample is heated. At RT the measured QY is lower because our model does not include dynamic effects. Relaxation brings the excited molecule faster to the conical intersection and thus enhances its decay. The fact that the experimental data lies below the line also at lower temperatures (close to 200 K), where our model gives excellent fits to the transient decay, suggests that the ultrafast picosecond decay process observed at RT[13−15] persists down to the glass

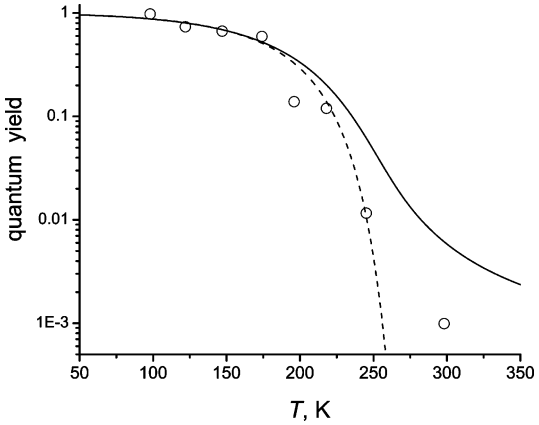

Figure 8. Temperature dependence of the fluorescence quantum yields for HBDI in a basic 0.5 mol fraction glycerol−water solution. Points were obtained from the area under the steady-state spectra reported in ref 37. Full and dashed lines are eqs 9 and 10, respectively, with the parameters of Table 1.

transition. This component is too fast to pick up with the TCSPC apparatus and should be probed by faster detection methods.

5. Discussion

We have presented fluorescence de-excitation data for *p*-HBDI, a model GFP Cro, in its anionic state, in viscous solvents, and over a wide temperature range. In agreement with Michel-Beyerle and co-workers,[12] we find multiexponential behavior that is strongly coupled to solvent viscosity. The complex-looking data were compared with a simple theoretical model for IC, depicting inhomogeneous kinetics with a nonlocal Gaussian sink term. The model has three temperature-independent parameters τ_f, A, and x_0. We have used for τ_f a value close to 3.3 ns, as was previously reported for wild-type GFP.[4] With a single temperature-adjustable parameter, b, excellent fits were obtained. Our fits encompass the full time evolution from the initial rising phase and up to long times. They reveal a linear dependence of b on $1/T$, eq 12. This means that the model depends on only four temperature-independent constants, A, x_0, b_0, and b_1. (In comparison, dozens of adjustable parameters would be required to fit all of our data to sums of exponentials). Thus the complex kinetics are actually surprisingly simple, at least in the static limit investigated herein.

The agreement with experiment indicates that our mathematical model is a good description of the physical reality. Yet the simple one-dimensional picture of strongly shifted and intersecting potential curves may be oversimplified. We discuss the merits and weaknesses of the one-dimensional picture and consider the physical interpretation of the model parameters and its possible extension to two dimensions.

5.1. One-Dimensional Picture. Our model depends on the two functions, $p(x)$ and $k(x)$, both having a Gaussian functional form. This form may arise in different ways. We have presented a one-dimensional derivation, for several reasons:

(a) It is simple and easy to follow.

(b) It extends the familiar (but unsuccessful) BFO model[25] by replacing its delta-function sink by a coordinate-dependent one.

(c) It extends the theory of radiationless transitions[35,36] to a hybrid case, where one degree of freedom is in the strong-coupling limit and the rest are weakly coupled.

(d) It relates to the model of ligand binding to heme proteins,[27−31] and demonstrates how $k(x)$ can sometimes be exponential[27−31] and other times Gaussian.[32]

(e) It explains why a Gaussian sink characterizes systems with very wide inhomogeneous broadening.

(f) It suggests that the ES potential is much steeper than the GS one, which is borne out by both the quantum chemistry calculations[21] (see the potential surfaces in Figure 1) and the experimental observation of transient line narrowing.[13−15]

A problem with this one-dimensional picture is in the shift of the ES potential $V_1(x)$. Such a shift is calculated for the neutral form of HBDI[21] but not for the anionic form. In fact, the ES well in Figure 1 is immediately above the GS one, showing no observable shift.

5.2. Identification of the Slow Coordinate. Which is the x-coordinate of our model? Several observations indicate that the potential as a function of x is flat in the GS, becoming much steeper in the ES:

(a) The wide inhomogeneous broadening, which arises from the initial equilibrium distribution in the GS;

(b) The adequacy of a Gaussian rather than an exponential form for the sink term, $k(x)$, see discussion of eq 4;

(c) The dynamic line narrowing observed in nonviscous solutions.[15]

These characteristics help identify x as the phenyl rotation angle, ϕ ($x = 0$ corresponds to $\phi = 90°$ whereas $x = x_0$ corresponds to the in-plane conformation, $\phi = 180°$ or $0°$). It is a rotation around a single bond in the GS and a nearly double bond in the ES (Figure 1), which explains the dramatic increase in the force constant.

The quantum mechanical calculations[21] for HBDI in water find that in the GS the rotation barrier in ϕ is only 17 kJ/mol, whereas it is 82 kJ/mol in ψ. In the ES the roles of the two bonds reverse, so that the rotation barriers become 100 and 11 kJ/mol for ϕ and ψ, respectively. Higher-level quantum calculations[22−24] show that the two exocyclic C−C bond lengths, rather than exhibiting double and single bond characters, are much closer to each other in the ES. Rotation around either one can now be nearly barrierless. However, the identity of the active mode in the ES depends on solvation effects. It is ϕ when the calculation is done in vacuo,[23] but it switches to ψ when the HBDI is solvated.[24] This is due to the fact that the GS energy increases substantially along ψ, leading to an intersection of the two surfaces. The latter observation is in qualitative agreement with the potentials in Figure 1.

This scenario is analogous to the situation in models for ligand binding to heme proteins.[27−32] There x is a "protein coordinate", whereas the GS and ES correspond to the bound and unbound states of the heme, respectively. To fit the data, a weaker force constant was assumed for the bound state, producing a wide conformational distribution. Concomitantly, a Gaussian sink term was found to perform better than an exponential one.[32]

5.3. Fast Mode. As pointed out by Agmon and Hopfield,[27,28] the nonlocal sink term in x can result from two-dimensional dynamics involving a slow and a fast mode, with an appropriate averaging over the fast mode.[29] Multidimensional effects were also suggested for stilbene isomerization[33] and HBDI decay.[15] For excited HBDI, libration in ψ becomes much more facile than in the GS due to the flatness of the ES potential along ψ (Figure 1). It assists IC by driving the system closer to the conical intersection. This is due *not* to the variation of the ES potential with ψ, which is nearly flat, but rather to the steep increase in the GS potential as a function of ψ. As noted above, the identification of ψ as the active mode that leads to the conical intersection is in agreement with high-level quantum chemistry calculations, provided that solvent effects are included.[24]

In myoglobin, motion of the unbound ligand does not change the porphyrin absorption wavelength, so that each conformation absorbs at a distinct wavelength. In contrast, here all of the conformations seem to emit at approximately the same wavelength. Correcting for a weak dependence of the radiative rate constant on frequency, we find the same inhomogeneous kinetics at all wavelengths (Figure 7). This may be due to motion in ψ, which modulates the emission frequency for each ϕ. Thus each x is itself characterized by an inhomogeneously broadened spectrum, so that the overall fluorescence spectrum is broad due to both static and dynamic effects.

The magnitude of $k(x)$ is dictated by a process of barrier crossing in the perpendicular direction, ψ, for fixed $\phi \equiv 90° + x45°$. From our analysis, it has the Arrhenius form in eq 13, where both the preexponential frequency factor and activation energy depend on x. With the aid of the potential in Figure 1, we can understand the x dependence of the frequency factor. It is small at $\phi = 90°$ ($x = 0$), where the potential in ψ is flat. It is largest for $\phi = 0°$ or 180° ($x = 2$), where there is a deeper well at $\psi = 0°$. This agrees with the negative sign of b_0 obtained from our analysis, which resulted in a sharp increase of the preexponential between $x = 0$ to $x = x_0$.

The x dependence of the activation energy is not clear from these surfaces, which have their point of closest approach at $\phi = 0°$, $\psi = 90°$. Thus one might expect to have the *smallest* barrier at x_0, contradicting our $k(x)$. This suggests that additional, nonelectronic effects may come into play as discussed below.

5.4. Phenyl Paddle. In a viscous solvent, one can imagine how the coupling to the solvent further enhances the variation of the activation energy with x. In the planar geometry ($\phi = 0°$) libration in ψ cannot move the phenyl ring, which presents its broad side to the direction of motion. In this case the phenyl is anchored to the solvent and only the imidazolone ring librates. However, when $\phi = 90°$ the phenyl ring is oriented with its narrow side in the direction of motion, so that it may swing around more easily with ψ. This "paddle orientation" effect results in a more facile approach to the conical intersection with the phenyl ring rotated out of plane. It may thus contribute to the ϕ-dependence of the activation energy, making it larger for a planar phenyl ring, in agreement with our form for $k(x)$.

5.5. Methyl Rotors. The two methyls on the imidazolone ring probably rotate nearly freely even in viscous solutions. These degrees of freedom supply a dense thermal bath of rotational states that couple to the IC. These modes can enhance the nonradiative transition by accepting the excess energy. To study this aspect, it may be interesting to synthesize an analogue without methyl substituents and compare its behavior to that of HBDI.

6. Conclusion

In the present work we have developed our understanding of HBDI photophysics in three stages. First, we showed that unlike small rigid aromatic dyes, which decay monoexponentially to their GS, the HBDI anion in viscous solvents shows marked nonexponential behavior over a wide temperature range. Second, we found that a simple inhomogeneous model with a Gaussian sink term achieves an excellent quantitative fit with only one adjustable parameter. Finally, we discussed the possible microscopic origins of the model, suggesting a two-dimensional picture similar to the one discussed by Agmon and Kosloff for stilbene isomerization.[33] The emerging scenario is that rotation of the phenyl paddle (ϕ) allows its more facile swinging (ψ) into orientations that are closer to the conical intersection.

The interest in HBDI arose originally because it is a model Cro for the GFP. The exceptionally rigid GFP structure[11] has at least two functions: (a) It helps keep the Cro in a planar cis conformation, as remote as possible from the conical intersection.[18] (b) It maintains a few internal water molecules that form intact one-dimensional hydrogen-bond networks ("proton wires") within the protein.[41] These are shown to play a pivotal role in proton conduction from/to the active site.[42,43]

Acknowledgment. We thank Christina Scharnagl for permission to use the potential surfaces in Figure 1 and Laren M. Tolbert for a gift of *p*-HBDI. This research was supported in part by the Israel Science Foundation (Grant No. 191/03) and the James-Franck German−Israel Program in Laser−Matter Interaction.

References and Notes

(1) Phillips Jr., G. N. *Curr. Opin. Struct. Biol.* **1997**, *7*, 821.
(2) Tsien, R. Y. *Annu. Rev. Biochem.* **1998**, *67*, 509.
(3) Zimmer, M. *Chem. Rev.* **2002**, *102*, 759.
(4) Lossau, H.; Kummer, A.; Heinecke, R.; Pöllinger-Dammer, F.; Kompa, C.; Bieser, G.; Jonsson, T.; Silva, C. M.; Yang, M. M.; Youvan, D. C.; Michel-Beyerle, M. E. *Chem. Phys.* **1996**, *213*, l.
(5) Ward, W. W.; Cody, C. W.; Hart, R. C.; Cormier, M. J. *Photochem. Photobiol.* **1980**, *31*, 611.
(6) McCapra, F.; Razavi, Z.; Neary, A. P. *J. Chem. Soc., Chem. Commun.* **1988**, 790.
(7) You, Y.; He, Y.; Burrows, P. E.; Forrest, S. R.; Petasis, N. A.; Thompson, M. E. *Adv. Mater.* **2001**, *12*, 1678.
(8) Niwa, H.; Inouye, S.; Hirano, T.; Matsuno, T.; Kojima, S.; Kubota, M.; Ohashi, M.; Tsuji, F. I. *Proc. Natl. Acad. Sci., U.S.A.* **1996**, *93*, 13617.
(9) Kojima, S.; Ohkawa, H.; Hirano, T.; Maki, S.; Niwa, H.; Ohashi, M.; Inouye, S.; Tsuji, F. I. *Tetrahedron Lett.* **1998**, *39*, 5239.
(10) He, X.; Bell, A. F.; Tonge, P. J. *FEBS Lett.* **2003**, *549*, 35.
(11) Helms, V.; Straatsma, T. P.; McCammon, J. A. *J. Phys. Chem. B* **1999**, *103*, 3263.
(12) Kummer, A. D.; Kompa, C.; Niwa, H.; Hirano, T.; Kojima, S.; Michel-Beyerle, M. E. *J. Phys. Chem. B* **2002**, *106*, 7554.
(13) Webber, N. M.; Litvinenko, K. L.; Meech, S. R. *J. Phys. Chem. B* **2001**, *105*, 8036.
(14) Litvinenko, K. L.; Webber, N. M.; Meech, S. R. *J. Phys. Chem. A* **2003**, *107*, 2616.
(15) Mandal, D.; Tahara, T.; Meech, S. R. *J. Phys. Chem. B* **2004**, *108*, 1102.
(16) Vengris, M.; van Stokkum, I. H. M.; He, X.; Bell, A. F.; Tonge, P. J.; van Grondelle, R.; Larsen, D. S. *J. Phys. Chem. A* **2004**, *108*, 4587.
(17) Klessinger, M.; Michl, J. *Excited States and Photochemistry of Organic Molecules*; VCH Publishers: New York, 1995.
(18) Voityuk, A. A.; Michel-Beyerle, M.-E.; Rösch, N. *Chem. Phys. Lett.* **1998**, *296*, 269.
(19) Voityuk, A. A.; Michel-Beyerle, M.-E.; Rösch, N. *Chem. Phys.* **1998**, *231*, 13.
(20) Weber, W.; Helms, V.; McCammon, J. A.; Langhoff, P. W. *Proc. Natl. Acad. Sci., U.S.A.* **1999**, *96*, 6177.
(21) Scharnagl, C.; Raupp-Kossmann, R. A. *J. Phys. Chem. B* **2004**, *108*, 477.
(22) Toniolo, A.; Olsen, S.; Manohara, L.; Martínez, T. J. *Faraday Discuss.* **2004**, *127*, 149.
(23) Martin, M. E.; Negri, F.; Olivucci, M. *J. Am. Chem. Soc.* **2004**, *126*, 5452.
(24) Altoe', P.; Bernardi, F.; Garavelli, M.; Orlandi, G.; Negri, F. *J. Am. Chem. Soc.* **2005**, *127*, 3952.
(25) Bagchi, B.; Fleming, G. R.; Oxtoby, D. W. *J. Chem. Phys.* **1983**, *78*, 7375.
(26) Austin, R. H.; Beeson, K. W.; Eisenstein, L.; Frauenfelder, H.; Gunsalus, I. C. *Biochemistry* **1975**, *14*, 5355.
(27) Agmon, N.; Hopfield, J. J. *J. Chem. Phys.* **1983**, *78*, 6947. Erratum: *J. Chem. Phys.* **1984**, *80*, 592.
(28) Agmon, N.; Hopfield, J. J. *J. Chem. Phys.* **1983**, *79*, 2042.
(29) Agmon, N.; Rabinovich, S. *J. Chem. Phys.* **1992**, *97*, 7270.
(30) Agmon, N.; Sastry, G. M. *Chem. Phys.* **1996**, *212*, 207.
(31) Agmon, N. *Biophys. J.* **2004**, *87*, 1537.
(32) Dantsker, D.; Samuni, U.; Friedman, J. M.; Agmon, N. *Biochim. Biophys. Acta* **2005**, *1749*, 234.
(33) Agmon, N.; Kosloff, R. *J. Phys. Chem.* **1987**, *91*, 1988.
(34) Hill, T. L. *An Introduction to Statistical Mechanics*; Addison-Wesley: Reading, MA, 1960.
(35) Siebrand, W. *J. Chem. Phys.* **1967**, *46*, 440.

(36) Englman, R.; Jortner, J. *Mol. Phys.* **1970**, *18*, 145.
(37) Stavrov, S. S.; Solntsev, K. M.; Tolbert, L. M.; Huppert, D. *J. Am. Chem. Soc.* **2006**, *128*, 1540.
(38) Press: W. H.; Flannery, B. P.; Teukolsky, S. A.; Vetterling, W. T. *Numerical Recipes: The Art of Scientific Computing*; Cambridge University Press: Cambridge, U. K., 1986.
(39) Lewis, J. E.; Maroncelli, M. *Chem. Phys. Lett.* **1998**, *282*, 197.
(40) Horng, M. L.; Gardecki, J. A.; Papazyan, A.; Maroncelli, M. *J. Phys. Chem.* **1995**, *99*, 17311.
(41) Agmon, N. *Biophys. J.* **2005**, *88*, 2452.
(42) Leiderman, P.; Huppert, D.; Agmon, N. *Biophys. J.* **2006**, *90*, 1009.
(43) Agmon, N. *Chem. Phys. Lett.* **2005**, *417*, 530.